Published in final edited form as:
Eur J Neurosci. 2008 March ; 27(6): 1353–1363. doi:10.1111/j.1460-9568.2008.06106.x.

Imbalance between excitation and inhibition among synaptic connections of CA3 pyramidal neurons in cultured hippocampal slices

Alberto Cruz-Martín and **Felix E. Schweizer**
Interdepartmental Ph.D. Program for Neuroscience, Department of Neurobiology and Brain Research Institute, David Geffen School of Medicine at UCLA, CHS 63-323, 650 Charles E. Young Drive South, Los Angeles, CA 90095-1763, USA

Abstract

A fundamental property of small neuronal ensembles is their ability to be selectively activated by distinct stimuli. One cellular mechanism by which neurons achieve this input selectivity is by modulating the temporal dynamics of excitation and inhibition. We explored the interplay of excitation and inhibition in synapses between pyramidal neurons of cornu ammonis field 3 of the hippocampal formation (CA3) in cultured rat hippocampal slices, where activation of a single excitatory cell can readily recruit local interneurons. Simultaneous whole-cell recordings from pairs of CA3 pyramidal neurons revealed that the strength of connections was neither uniform nor balanced. Rather, stimulation of presynaptic neurons elicited distinct combinations of excitatory postsynaptic current–inhibitory postsynaptic current (EPSC–IPSC) amplitudes in the postsynaptic neurons. EPSC–IPSC sequences with small EPSCs had large IPSCs and sequences that contained large EPSCs had small IPSCs. In addition to differences in the amplitudes of the responses, the kinetics of the EPSCs were also different, creating distinct temporal dynamics of excitation and inhibition. Weaker EPSCs had significantly slower kinetics and were efficiently occluded by IPSCs, thereby further limiting their contribution to depolarizing the postsynaptic membrane. Our data suggest that hippocampal pyramidal cells may use an imbalance between excitation and inhibition as a filter to enhance selectivity toward preferential excitatory connections.

Keywords

excitatory postsynaptic current; feed-forward inhibition; inhibitory postsynaptic current; network connectivity; rat; timing

Introduction

Direct excitatory and inhibitory connections between two neurons form the basis of neuronal networks. The study of these monosynaptic connections in acute, cultured brain slices and primary neuronal cultures has contributed much to our understanding of neuronal connectivity and has led to the proposal that excitatory and inhibitory connections onto a

Correspondence: Dr Felix E. Schweizer, as above. felixs@ucla.edu.

Supplementary material
The following supplementary material may be found on http://www.blackwell-synergy.com
Fig. S1. EPSCs of smaller amplitudes are more efficiency occluded than their larger counterparts.
Please note: Blackwell Publishing are not responsible for the content or functionally of any supplementary materials supplied by the authors. Any queries (other than missing material) should be directed to the correspondence author for the article.

neuron should be balanced (Turrigiano & Nelson, 2004) and, together with intrinsic properties (MacLean *et al.*, 2003), will set the appropriate rate of action potential (AP) firing (Toyoizumi *et al.*, 2005). Such a balance appears particularly important when considering ensembles of neurons that can form recurrent networks, where excitation could easily become dominant and therefore lead to hyperexcitability. One of the simplest circuits is an excitatory–inhibitory feed-forward network, which is composed of incoming excitatory axons that synapse onto principal cells and interneurons that provide local inhibition (Buzsaki, 1984; Miles, 1990; Karnup & Stelzer, 1999; Gabernet *et al.*, 2005; Mittmann *et al.*, 2005). Activation of this simple network will result in a brief period of monosynaptic excitation of the postsynaptic principal cell that is quickly dampened by the disynaptic inhibitory component (Debanne *et al.*, 1995). In the neocortex and hippocampus, the timing between activation of excitatory and inhibitory inputs is crucial for synaptic integration, as most unitary excitatory postsynaptic potentials (EPSPs) are not strong enough to depolarize the principal cell above threshold (Miles & Wong, 1986; Pavlidis & Madison, 1999; Holmgren *et al.*, 2003) and many EPSPs must be temporally integrated in order to trigger an AP. Feed-forward inhibition imposes an additional constraint by counteracting depolarization, especially when the latter is caused by late unitary EPSPs. Such feed-forward networks are thus characterized by a narrow window of opportunity (Lloyd, 1946), or integration window, where the most synchronized unitary EPSPs can contribute to excitation of the postsynaptic target (Pouille & Scanziani, 2001; Gabernet *et al.*, 2005).

Together with Hebbian plasticity, independent modulation of excitation and inhibition could thus provide a powerful means for neural networks to establish preferential synaptic connections among its cells to focus on different types of information. Opposing signs of short-term plasticity at excitatory and inhibitory synapses have been reported to make feed-forward connections more sensitive to high-frequency bursts of APs (e.g. Klyachko & Stevens, 2006). Interestingly, induction of long-term potentiation in excitatory synapses without concurrent enhancement in inhibitory synapses results in degradation in the temporal precision of the AP (Lamsa *et al.*, 2005). One complicating factor in such experiments is that they rely on extracellular stimulation, which recruits many axons. The resulting postsynaptic measurement thus represents an average over anatomically distinct pathways. This obscures the underlying behavior of elementary physiological building blocks and could miss important aspects of information processing and network behavior.

Simultaneous whole-cell recordings from cornu ammonis field 3 of the hippocampal formation (CA3) pyramidal cells have shown that there is great variability in the amplitude of the evoked excitatory postsynaptic current (EPSC), the likely source of this variability arising from differences in the number of synapses across connected cells (Pavlidis & Madison, 1999). The CA3 region provides an excellent setting in which to explore the relationship between excitation and inhibition because of its high probability of synaptic connectivity (Pavlidis & Madison, 1999) and the ability of a single pyramidal cell to recruit local interneurons upon its activation (Debanne *et al.*, 1995, 2006). In this small circuit comprised of two neighboring pyramidal cells and their local interneurons, we now describe the heterogeneity of combined excitatory and inhibitory currents and their temporal dynamics.

Materials and methods

Organotypic slices

Organotypic slices from rat hippocampus were prepared using an interface method (Stoppini *et al.*, 1991) following procedures approved by the UCLA Institutional Animal Care and Use Committee. Briefly, Sprague-Dawley rats (6–8 days old) were anesthetized with halothane, decapitated and the brains were quickly removed and placed in an ice-cold

minimum essential medium (Gibco, Invitrogen, Carlsbad, CA, USA) based slicing solution containing (in mM): 3.0 $MgSO_4$, 10.0 glucose, 2.5 HEPES and 10.0 Tris-base (pH 7.2). The hippocampi were dissected and sliced into 400 μm thick coronal sections using a vibratome (VT-1000, Leica Microsystems, Wetzlar, Germany). Slices were then transferred into a Millicell-CM (Millipore, Billerica, MA, USA) in a well of a six-well plate containing 1 mL of culture medium. The culture medium consisted of Eagle's minimum essential medium (Media Tech, Manassas, VA, USA) supplemented with (in mM): 0.55 $CaCl_2$, 1.85 $MgSO_4$, 25.5 glucose, 30 HEPES, 0.5 ascorbic acid, 1 glutamine, as well as 1% penicillin/streptomycin and 20% horse serum. Slices were incubated in 5% CO_2 at 37ºC for 6–12 days prior to experiments. Culture medium was changed 1 and 24 h after culturing, and every other day thereafter.

Electrophysiology

Organotypic slices were transferred to a recording chamber on the stage of an upright microscope (Carl Zeiss, Oberkochen, Germany) and viewed through a 40× water-immersion lens using differential interference contrast optics or epifluorescence. Slices were continually superfused at room temperature (21–23ºC) with artificial cerebrospinal fluid composed of (in mM): 119 NaCl, 3 KCl, 2 $MgSO_4$, 2 $CaCl_2$, 26 $NaHCO_3$, 11 glucose, 1 Na_2HPO_4 and CGP 52432 ($GABA_B$ antagonist; 3 μm), pH 7.3, 310 mOsm. Whole-cell recordings were obtained using patch electrodes (2–4 MΩ) pulled from thin-walled borosilicate glass capillaries (World Precision Instruments, Sarasota, FL, USA) and filled with an intracellular solution containing (in mM): 120 K-gluconate, 30 HEPES, 5 $MgCl_2$, 0.6 EGTA, 10 Na_2-creatine phosphate, 5 Na-ATP, 0.6 Na-GTP, pH 7.2. Alexa-594 (25 μM) (Molecular Probes, Eugene, OR, USA) was added to the intracellular solution for some experiments. An uncorrected liquid junction potential of 13.6 mV was calculated using the Liquid Junction Potential Calculator integrated in pClamp (Molecular Devices, Sunnyvale, CA, USA). Simultaneous whole-cell recordings were obtained using an Axon Instruments Multiclamp 700A amplifier (Molecular Devices, Sunnyvale, CA, USA) and custom software developed in LabView (National Instruments, Austin, TX, USA). Pre-and postsynaptic signals were filtered at 10 or 2 kHz, respectively, and sampled at 25 kHz. Pyramidal cells were identified based on their localization in the pyramidal cell body layer, their morphology including apical and basolateral dendrites (Fig. 1A) and their firing properties, i.e. their ability to accommodate in response to long depolarizing current injections (≥ 500 ms). Synaptic connections between adjacent pyramidal cells (cell bodies closer than 100 μm) were assessed by inducing a pair of APs (95 ms interstimulus interval; Fig. 1D) in the presynaptic current-clamped cell after injecting a brief (2 ms) depolarizing current (600 pA). In connected pairs, presynaptic APs generated EPSCs in the neighboring voltage-clamped neuron. If the membrane of the postsynaptic cell was taken to V_m close to −50 mV (−49.51 ± 0.04 mV, n = 29), we observed that in about half of the pairs (29 of 60 pairs) the EPSC was followed by a brief inhibitory (outward) postsynaptic current (IPSC), consistent with a monosynaptic excitatory and a disynaptic inhibitory connection (see below). The remainder of the paired recordings failed to reveal any inhibitory contribution and thus probably represented pure monosyn-aptic excitatory connections. For this study, we focused on those pairs where the inward EPSC was followed by an outward IPSC. The outward component of the EPSC–IPSC (E–I) sequence was blocked by the $GABA_A$ inhibitor picrotoxin (100 μM) but the treatment increased the spontaneous excitatory activity in the slice such that reliable amplitude measurements were not possible. After voltage-clamp recordings, postsynaptic cells were held under current-clamped conditions to characterize their AP firing properties. Passive membrane properties (R_{in}, 92.0 ± 4.7 MΩ, n = 29) of the cell were monitored regularly during the recordings. Series resistance was usually below 10 MΩ (8.3 ± 0.6 MΩ, n = 29) and compensated by 50–70%. Experiments were the series resistance changed by more than 20% over the time course of the experiment were not used in the data set.

Determination of excitatory and inhibitory conductances

Due to the susceptibility of organotypic cultures to epileptic seizures (Debanne *et al*., 2006) the EPSC could not be isolated and reliably measured by pharmacologically blocking the IPSC. Instead, isolation of individual excitory and inhibitory components of an E-I sequence recorded at V_m~−50 mV was accomplished offline by taking the pure EPSC recorded at E_{rev} IPSC (−58.7 ± 0.6 mV, n = 29), determined from the I–V curve (see Fig. 2B and C), and scaling it to −50 mV to take into account the reduced driving force:

$$I_{scaled}(V_m, t)=(V_m - E_{rev})/(E_{rev}IPSC - E_{rev}) * I(E_{rev}IPSC, t)$$

in which V_m is the holding potential (−49.5 ± 0.1 mV, n = 29) and E_{rev} is the reversal potential for the EPSC (4.5 ± 0.5 mV, n = 29, determined from the I–V curve, see Fig. 2B and C). This scaled EPSC was then arithmetically subtracted from the E–I sequence with the resulting current being equal to the IPSC (Fig. 2D). To obtain synaptic conductances we used the following equation:

$$g_{syn}(t)=I(t)/(V_m - E_{rev})$$

in which I(t) is either the EPSC or the IPSC at V_m (~−50 mV) and E_{rev} represents the corresponding reversal potentials. The Erev IPSC (−58.7 mV) is in line with previously published numbers for acute slices (−47 mV at p5–10 and −73 mV at p20 (Banke & McBain, 2006) and is similar to the chloride equilibrium potential calculated using the Nernst equation (−64.4 mV).

Recording the EPSC at E_{rev} IPSC obviously does eliminate current flowing through the $GABA_A$ receptors but their opening will still increase the membrane conductance. Under current-clamp conditions this increased ‘shunt’ would diminish the amplitude of the excitatory component. However, in voltage clamp by definition there is no current flowing through the $GABA_A$ receptors at E_{rev} IPSC, no ‘shunting inhibition’ is present and all of the current flows through the other conductances present. The voltage escape due to the presence of uncompensated series resistance will produce some driving force. However, assuming 5 MΩ of uncompensated series resistance (Rs) and a peak excitatory current of 200 pA (see, e.g. Fig. 3A) the voltage escape will be maximally 1 mV. Together with the 6 nS inhibitory conductance (e.g. Fig. 4D) this would reduce the excitatory current maximally by 6 pA. Smaller synaptic currents generate less of a voltage escape and thus produce even less ‘shunting’ current. This does not take into account the difference in time course between the two conductance changes, which further minimizes the potential ‘shunting’ current. Recording at E_{rev} IPSC thus gives an accurate measure of the excitatory current without inhibitory contributions.

Miscellaneous

IGOR Pro 5.0 (WaveMetrics, Portland, OR, USA) and Origin 7.0 (OriginLab, Northampton, MA, USA) were used for data analysis and graphing. In most experiments, resampling statistics were used to determine the statistical significance in differences of means. Detailed analysis of the distribution of E–I sequences (Fig. 2) was accomplished by splitting the data into three groups (see Results) and performing a one-way anova and a planned comparison (Bonferroni test) to test for differences between pairs of groups. Data are expressed as mean ± SEM and significance was set at $P < 0.05$. For ‘Box and whiskers’ graphs, the lower and upper sides of the box indicate SEM, horizontal line inside boxes is median, symbol inside boxes is average, and whiskers are 10–90% of the values. For linear correlation the solid line is the least-squares fit to the data and dotted lines are 95% confidence intervals. To

determine a linear correlation between two variables the Pearson correlation coefficient (*R*) was calculated, this correlation was considered significant if $P < 0.05$.

Unless otherwise noted, reagents were obtained from Sigma-Aldrich (St Louis, MO, USA), except for CGP 52432 and 6,7-dinitroquinoxaline-2,3-dione (Tocris, Ellisville, MO, USA), and picrotoxin (EMD Biosciences, Madison, WI, USA).

Results

Lack of correlation between excitation and inhibition in E–I sequences

Neurons in cultured hippocampal slices were visualized using infrared differential interference contrast bright-field microscopy and were identified as pyramidal if they were located in the pyramidal cell layer and had a large, triangular cell shape with a prominent apical dendrite. Cells were also routinely filled through the patch pipette with the fluorescent dye Alexa-594 (25 μM) to better reveal the structure of the dendritic tree. Fig. 1A shows a maximal intensity projection of a z-stack of 15 two-photon images taken at 3 μm intervals at the end of the recording. We further confirmed their identity after whole-cell patching by the spiking pattern generated upon injection of depolarizing current pulses during current clamp (Fig. 1B and Table 1). Pyramidal cells exhibited regular spiking patterns of APs that accommodated during the current injection. Connected pairs were characterized by postsynaptic potentials elicited by the APs (Fig. 1B, arrow). Whole-cell voltage-clamp recordings from single CA3 pyramidal cells revealed spontaneous synaptic currents that were both inward and outward at a holding potential of −50 mV (Fig. 1C). At voltages close to −50 mV, currents through glutamate receptors are inward, whereas currents through $GABA_A$ receptors are outward. Indeed, many currents were biphasic with an early inward component followed by a somewhat slower outward current. To further explore the nature of these synaptic currents, we simultaneously recorded from pairs of neurons, holding one under current clamp at the cell's resting membrane potential (−59.48 ± 0.96 mV, $n = 29$) and holding the other under voltage-clamp close to −50 mV to enable the recording of synaptic currents. A brief current injection into the current-clamped neuron was used to trigger an AP, which elicited a postsynaptic current in the voltage-clamped postsynaptic cell if the two neurons were synaptically connected (Fig. 1D). These evoked postsynaptic currents, which could be blocked by addition of 6,7-dinitroquinoxaline-2,3-dione to the extracellular bath solution (Fig. 1E), were frequently a mixture of an early inward current followed by a later outward current, much like the spontaneous currents (Fig. 1C). The initial delay of the inward current measured from the peak of the presynaptic AP was 1.64 ± 0.10 ms ($n = 29$), indicating a monosynaptic connection between the two neurons (Miles & Wong, 1986; Debanne *et al*., 1995; Pavlidis & Madison, 1999). Generation of these mixed responses in the postsynaptic cell indicated that activation of a presynaptic cell activates a simple circuit composed of incoming excitatory synapses that activate neighboring postsynaptic pyramidal cells and local interneurons, which provide feed-forward inhibition.

The interaction of excitation and inhibition enhances the segregation of E–I responses

We next wanted to investigate the relationship and variation of these mixed excitatory and inhibitory (E–I) responses within individual neighboring cells in a network. Even though their temporal interactions and functionality have been extensively described (Pouille & Scanziani, 2001; Gabernet *et al*., 2005), many of these experiments have relied on extracellular stimulation, which is experimentally easier but will recruit a population of axons. The elicited postsynaptic currents may thus represent an average over anatomically distinct pathways, which could obscure the variability and temporal interaction between these responses.

Recent studies have shown that, due to the susceptibility of organotypic cultures to epileptic seizures (Debanne *et al.*, 2006), the EPSC cannot be reliably isolated and measured by pharmacologically blocking inhibitory postsynaptic currents. We therefore recorded the mixed postsynaptic currents at the resting membrane potential (V_m; Fig. 2D, black line) and at the reversal potential of the IPSC (E_{rev} IPSC), where the IPSC is by definition zero. To obtain the EPSC at V_m (Fig. 2D, dotted line), we scaled the 'pure' EPSC (measured at E_{rev} IPSC) to account for the difference in driving force [scale factor: ($V_m - E_{rev}$ EPSC)/(E_{rev} IPSC) E_{rev} EPSC) ~ 0.85]. Finally, to obtain the IPSC at V_m (Fig. 2D, gray line), we subtracted the scaled EPSC (Fig. 2D, dotted line) from the recorded current (Fig. 2D, black line). The reversal potentials for the excitatory and inhibitory currents were determined by recording the responses at different holding potentials (Fig. 2B) and measuring the current amplitude early and late in the trace (Fig. 2B). Plotting these values against the voltage yielded relatively linear I–V plots (Fig. 2C) and voltages at which the curves intersect the abscissa were taken as the respective reversal potentials (E_{rev} EPSC, 4.50 ± 0.48 mV; E_{rev} IPSC, −58.67 ± 0.56 mV, n = 29; Fig. 2A–C and Materials and methods).

Plotting the average peak amplitude of the 'pure' EPSC against the 'pure' IPSC (Fig. 2E) indicated that the combinations were not random (no correlation) and neither did they show a positive correlation, as expected if they were balanced (Wehr & Zador, 2003). Instead, we observed that the E–I sequences for the population of cells recorded exhibited an L-shaped distribution (Fig. 2E). In this distribution one side of the 'L' contained larger amplitude EPSCs that tended to associate with IPSCs of smaller amplitudes. At the other side of this distribution we could observe the weak inputs, which contained small amplitude EPSCs that were followed by large amplitude IPSCs.

We next observed how excitation and inhibition interact at V_m close to −50 mV, where enough driving force exists to generate postsyn-aptic currents for both components. For this we plotted the measured (rather than the calculated 'pure') peak inward current against the measured peak outward current in the E–I sequence and again observed an L-shaped distribution (Fig. 2F). Indeed, the segregation of strong and weak inputs was further enhanced (Fig. 2E) when compared with the 'pure' components (Fig. 2A). Thus, taking into account the temporal interaction between excitation and inhibition not only conserved but also accentuated the two categories of connections, demonstrating that the underlying imbalance between excitation and inhibition is effective in functional neuronal circuits. We investigated this interaction further by analysing the kinetics of excitation and inhibition.

The temporal interactions of excitation and inhibition are distinct between weak and strong inputs

In order to facilitate the analysis, we divided the dataset into two groups based on the median value of the pure EPSCs (Fig. 2E), which dissected the L-shaped distribution close to the vertical arm and generates these two groups of E–I sequences: neuronal pairs with an EPSC more negative than −32.57 pA were assigned to the 'strong' group, whereas pairs with EPSCs less negative than −32.57 pA were called 'weak'. (EPSC amplitude: weak, −15.39 ± 2.26 pA, n = 15; strong, −86.69 ± 13.69 pA, n = 14, $P < 0.05$; IPSC amplitude: weak, 83.17 ± 17.94 pA, n = 15; strong, 27.32 ± 6.98 pA, n = 14, $P < 0.05$.) Importantly, both types of connections were routinely found in the same slice and we did not observe a developmental change in the proportion of weak vs. strong connections (6 vs. 12 days *in vitro*; data not shown), making it unlikely that they simply represent two developmental stages. In addition to analysing the data grouped on either side of the median, we also determined whether there was a correlation between a given metric and the amplitude of the 'pure' EPSC.

Linear summation with IPSCs will effectively weaken EPSCs. We determined how large the amplitude of the EPSCs measured at −50 mV was compared with the amplitude of the 'pure' EPSCs scaled from the one measured at E_{rev} IPSC (see above). If inhibition and excitation were balanced, there should be no difference in this metric between strong and weak pairs and no correlation with the amplitude of the 'pure' EPSC. However, weak inputs deviated more than strongly than strong inputs (weak: 38.97 ± 6.38%, n = 15; strong: 83.23 ± 3.67%, n = 14, $P < 0.05$; Fig. 3A). These results show that EPSCs of smaller amplitudes were more efficiently occluded than their larger counterparts (see Supplementary material, Fig. S1). One mechanism to account for this discrepancy might lie in differences in the kinetics of either the EPSC or the IPSC (Wilent & Contreras, 2005). EPSCs with slower kinetics will be more efficiently occluded by a polysynaptic IPSC than their faster counterparts. As a result of this temporal interaction, faster EPSCs will contribute more to the excitation of the postsynaptic membrane before finally being quenched by inhibition. Measurements of the kinetics of the EPSCs for both groups of responses show that indeed EPSCs of the weak inputs had slower rise times and longer synaptic delays than the EPSC of the strong inputs (20–80% rise time: weak, 1.43 ± 0.18 ms, n = 15; strong, 0.81 ± 0.07 ms, n = 14, $P < 0.05$; Fig. 3B and C; synaptic delay EPSC: weak, 2.77 ± 0.37 ms, n = 15; strong, 1.68 ± 0.14 ms, N = 14, P-value < 0.05; plot not shown). As the rise time is more difficult to measure for small events, we also determined the maximal slope for both groups and obtained similar results (maximum slope: weak, −41.9 ± 5.2 pA/ms, n = 15; strong, −133 ± 20 pA/ms, n = 14, $P < 0.05$). There was no difference in the kinetics of the IPSC between the two inputs (20–80% rise time: weak, 1.47 ± 0.09 ms, n = 15; strong, 1.52 ± 0.08 ms, n = 14, $P = 0.67$; synaptic delay IPSC: weak, 4.08 ± 0.17 ms, n = 15; strong, 4.2 ± 0.15 ms, n = 14, $P = 0.55$), suggesting that this temporal interaction is mainly regulated by the kinetics of the EPSC.

In agreement with our measurements from voltage-clamped currents, isolation of excitatory and inhibitory conductances for weak and strong inputs also showed a similar relationship between their peak amplitudes (Fig. 4A and B; weak: g max_{EPSC} 0.27 ± 0.05 nS, n = 15; strong: 1.38 ± 0.23 nS, $\underline{n}$ = 14, $P < 0.05$). Weak inputs had larger inhibitory conductances than their stronger counterparts (g max_{IPSC}: weak, 6.42 ± 1.04 nS, n = 15; strong, 3.56 ± 0.83 nS, n = 14, $P < 0.05$; Fig. 4C and D). This relationship resulted in strong inputs having larger excitation to inhibition ratios (g_{EPSC}: g_{IPSC}: weak, 0.07 ± 0.02, n = 15; strong, 0.57 ± 0.15, n = 14, $P < 0.05$; Fig. 4E).

To investigate whether stronger inputs also allowed for a potentially longer 'window of opportunity' (Lloyd, 1946), or integration window, where the most synchronized unitary EPSPs can contribute to excitation of the postsynaptic target (Pouille & Scanziani, 2001; Gabernet *et al.*, 2005), we plotted the integration window against the values for g_{EPSC}: g_{IPSC}. The integration window was measured as the time between activation of the inward, excitatory current and the time when the total current becomes outward, i.e. hyperpolarizing. As shown in Fig. 4F, there is a strong positive correlation between these measures (R = 0.78, $P < 0.05$; n = 29). Furthermore, superimposition of the isolated excitatory and inhibitory conductance traces also revealed that EPSCs at weak inputs were more efficiently occluded by the IPSCs than at strong inputs (Fig. 5A and B). Taken together these data suggest that an imbalance between excitation and inhibition can be used between synaptic neighbors to regulate their contribution to excitation of the postsynaptic cell.

To determine whether our data contain two different populations or might be more consistent with a continuum, we compared the rise times of the EPSCs for the extreme values, the lower and upper thirds, within the L-shaped distribution. These sub-groups were comprised of the weakest and strongest EPSCs in the graph, excluding the middle values. We found that, as expected, the stronger EPSCs had faster rise times than the weaker EPSCs

(20–80% rise time: weak, 1.56 ± 0.28 ms, $n = 9$; strong, 0.73 ± 0.10 ms, $n = 9$; Bonferroni test, $P < 0.05$). In addition, we found that, although these two groups differ in their kinetics, they were not different when they were individually compared with the remaining middle group (20–80% rise time: weak, 1.56 ± 0.28 ms, $n = 9$; middle, 1.10 ± 0.38 ms, $n = 11$; Bonferroni test, $P > 0.05$; 20–80% rise time: strong, 0.73 ± 0.10 ms, $n = 9$; middle, 1.10 ± 0.38 ms, $n = 11$; Bonferroni test, $P > 0.05$). Thus, our data probably represent a continuum with the two extremes dominating the distribution. It is interesting to speculate that the 'middle' group might be composed of connections poised to join either group. However, they might be dedicated to either behavior as their inclusion in the analysis maintains a bimodal behavior.

AP properties suggest that weak and strong inputs target the same postsynaptic target

A possible explanation for the segregation of weak and strong synapses in the CA3 region could be that they target different types of postsynaptic pyramidal cells. These targets will then determine the properties of the excitatory and inhibitory synapses (Reyes *et al.*, 1998; Atwood & Karunanithi, 2002). However, measurements of the amplitude, half width, maximal rate of depolarization and repolariza-tion of APs were not different between the two (Table 1). In addition, the accommodation ratio and frequency of APs elicited with a positive current injection were the same (Table 1).

Although we did not find evidence for weak and strong inputs contacting different postsynaptic targets, the segregation of inputs might be a result of a more global cellular mechanism that adjusts excitation and inhibition depending on the history of activity of the cell (Maffei *et al.*, 2004). In this scenario, postsynaptic cells could be in different states that determine which types of inputs they will receive. If this were true, then we would expect that, due to homeostatic mechanisms, a cell that had low levels of activity might receive spontaneous EPSCs that are stronger on average than a cell that had high levels of activity. However, the frequency and amplitude of spontaneous EPSCs were the same between postsynaptic cells that receive weak and strong inputs (weak vs. strong; frequency: 5.38 ± 1.12 Hz, $n = 10$, 5.69 ± 1.20 Hz, $n = 10$, $P = 0.84$; amplitude: −45.58 ± 4.78 pA, $n = 10$, −43.80 ± 4.88 pA, $n = 10$, $P = 0.79$; Fig. 6A–C), suggesting that the postsynaptic cells that we recorded from might have been exposed to similar levels of activity. Values for rise times of spontaneous activity were also the same for postsynaptic cells that weak and strong inputs contacted (weak vs. strong: 2.05 ± 0.24 ms, $n = 10$; 2.14 ± 0.17 ms, $n = 10$, $P = 0.74$; Fig. 6D). These results also suggest that the postsynaptic cells studied belong to a homogeneous population of pyramidal cells (Fig. 1A and B). Intriguingly, when analysing the spontaneous EPSCs in individual postsynaptic cells, we often (eight out of 20) found an L-shaped distribution when rise times were plotted against peak amplitude values of the EPSC (Fig. 6E). This supports our conclusion that individual connections onto postsynaptic pyramidal neurons do segregate into two groups representing either weak or strong connections.

Discussion

Using simultaneous whole-cell pair recordings from connected CA3 pyramidal neurons, we have explored the dynamics of excitation and inhibition in cultured slices. We find that excitation and inhibition do not scale together but are also not independent of each other. Rather, we observe a dominance of either excitation or inhibition; strong monosynaptic EPSCs are accompanied by weak feed-forward inhibition, whereas weak EPSCs are additionally weakened by strong feed-forward inhibition. This relationship is evident as an L-shaped distribution when the mean amplitudes of the inhibitory and excitatory components of the postsynaptic responses, measured in 29 connected pairs, are plotted against each other (Fig. 2). Comparison of mean excitatory and inhibitory currents for pure

and mixed responses shows that, at a membrane potential close to −50 mV, where both currents interact, the L-shaped distribution is accentuated. This behavior is a direct result of the EPSC being occluded by the IPSC. Interestingly, weak EPSCs are more efficiently occluded than strong EPSCs. As a possible mechanism for such preferential occlusion, we observed that weaker EPSCs had slower kinetics than stronger EPSCs. Therefore, weak excitatory conductances are activated more synchronously with inhibitory conductances. Consequently, inhibition is actively limiting the contribution of weak EPSCs to excitation of the postsynaptic membrane. Thus, connections between these excitatory neurons are, in effect, either excitatory or inhibitory.

The difference between slow/weak and fast/strong connections could conceivably be due to differences in the postsynaptic target neuron (Atwood & Karunanithi, 2002). For example, in layer II/III of rat somatosensory cortex the synapses of an individual pyramidal cell will differ in their strength, short-term plasticity and intracellular calcium dynamics depending on the type of postsynaptic target that their presynaptic boutons contact (Reyes *et al.*, 1998; Koester & Johnston, 2005). In addition, evidence for the existence of distinct types of pyramidal cells has been found in the forebrain (Sugino *et al.*, 2006) and cortical sub-networks composed of pyramidal cells with different firing properties, branching patterning and synaptic connections have been identified (Wang *et al.*, 2006). However, our data are more consistent with a homogeneous class of postsynaptic neurons receiving distinct presynaptic inputs, as: (i) we failed to detect a difference in AP properties and firing patterns of the postsynaptic neurons, and (ii) in a large proportion (~40%) of neurons, spontaneous postsynaptic responses were also a mixture of fast/large and small/slow responses. An anatomical explanation for the difference in EPSC kinetics might be that excitatory synapses from weak and strong inputs are segregated along the somato-dendritic axis of the neuron. Excitatory synapses of strong inputs might be located more proximal to the soma, whereas weaker inputs connect at more distal places along the dendrite. As a result, the kinetics of the EPSCs and the temporal dynamics of excitation and inhibition would be dictated by the electrotonic propagation of excitatory inputs to the soma. Alternatively, the weak and strong inputs might signal to AMPA receptors with different sub-unit compositions (Geiger *et al.*, 1997) or might have distinct time courses of neurotransmitter release (Geiger *et al.*, 1997; Schweizer *et al.*, 1998).

Although we did not find evidence for heterogeneity in the postsynaptic pyramidal cell type, the neurons could exist in different states that are modulated based on their history of activity. Their previous activity levels could then regulate how much excitation and inhibition they receive, and thus lead to the segregation of strong and weak inputs. For example, experiments in primary visual cortex of rat have shown that 2 days of visual deprivation early in life can massively increase the amount of spontaneous activity in pyramidal cells, mainly due to an increase in excitatory and a concomitant decrease in inhibitory synaptic drive (Maffei *et al.*, 2004). However, our data of spontaneous EPSCs show that a more global mechanism adjusting excitatory and inhibitory inputs might not be playing a role as measurements of the rise time, amplitude and frequency of EPSCs were not different for the two groups, although in many cells two kinetically distinct inputs could be detected. A more plausible explanation for our results is that the segregation of weak and strong inputs reflects the individual activity history of synapses and possibly the competition between them. Excitatory synapses that end up contributing more to the excitation of the postsynaptic cell are rewarded with less feed-forward inhibition, whereas their weaker counterparts are further inhibited (Tao & Poo, 2005; Lien *et al.*, 2006).

One important point of discussion relates to whether these are two distinct populations or a continuum. Based on the visual inspection of the L-shaped distribution of postsynaptic currents, we divided the data using a cut-off value for the amplitude of the inward currents.

Setting this limit seemed a reasonable approach for our analysis, as by dividing the two sides of this 'L' we captured the essence of this segregation. It also allowed for the comparison of synaptic parameters between these two cases without arbitrarily excluding any data. However, the L-shaped distribution of the postsynaptic currents is just as likely to indicate a continuum of E–I sequences that reaches an extreme at each end of this distribution (Fig. 2A and E). One side of this extreme contains mixed E–I feed-forward responses, which behave like an excitatory current, whereas the other mainly conveys inhibition. A very significant consequence of such an L-shaped distribution of responses is that the population average of the EPSC and IPSC amplitude yields an average connection behavior that is not represented in the actual data set (Golowasch *et al.*, 2002). As extracellular stimulation of fibers, as frequently used in the field, will recruit a mixture of connections along this L-shaped distribution, the measured postsynaptic response will represent the average behavior of that mixture with no relationship to any of the inputs actually present. This will probably affect the filtering properties of neuronal networks present in hippocampal slices (Klyachko & Stevens, 2006) and the physiological paradigms for long-term plasticity (Lamsa *et al.*, 2005).

Interestingly, brief periods of epileptiform activity in CA3–CA3 synapses, elicited by bath application of bicuculline methochloride, can strengthen excitatory synapses and relieve the EPSP from its occlusion by inhibition (Debanne *et al.*, 2006). This process depends on *N*-methyl-d-aspartate receptors and is occluded by long-term potentiation (Debanne *et al.*, 2006). Competition between excitatory synapses and the subsequent segregation of inputs could then be established using a Hebbian mechanism of synaptic plasticity, with feed-forward inhibition adjusting accordingly to make excitation more or less efficient.

The temporal dynamics of excitation and inhibition have been shown to be important in establishing stimulus selectivity for thalamo-recipient neurons in layer 2/3 of the rat barrel cortex (Wilent & Contreras, 2005). Some of the thalamo-recipient neurons have been shown to be sensitive to the angular direction of whisker deflection (Simons & Carvell, 1989). In these cells, excitatory synaptic conductances generated in the postsynaptic cell precede inhibitory conductances for the preferred direction of whisker deflection and, as the direction of whisker deflection deviates more from the preferred, inhibitory conductances overlap more with excitatory conductances. As a result, synaptic responses of thalamo-recipient neurons elicited by the direction of whisker deflection were associated with a systematic shift in the temporal relation of excitation and inhibition (Wilent & Contreras, 2005). In a similar manner, the dominance of either excitatory or inhibitory inputs in combination with their temporal dynamics could be used by CA3 pyramidal cells as a strategy to establish preferential connections.

Supplementary Material

Refer to Web version on PubMed Central for supplementary material.

Acknowledgments

We would like to thank Dean Buonomano, Jack Feldman, Fredrick Gregory, Thomas O'Dell, Ricardo Mostany and Kristen Willeumier for their comments and ideas, Gabriela David for help in the preparation of organotypic slices, and Peyman Golshani for his comments and help in the programming of the data analysis software. We would also like to thank Carlos Portera-Cailliau for his comments, ideas and the use of the two-photon microscope. This work was supported in part by NIH DC007678 (to F.E.S.), the NASA Harriett G. Jenkins Fellowship (JPFP to A.C.-M.) and the Achievement Rewards for College Scientists (ARCS) Foundation (to A.C.-M.).

Abbreviations

AP	action potential
CA3	cornu ammonis field 3 of the hippocampal formation
E–I	excitatory postsynaptic current–inhibitory postsynaptic current
EPSC	excitatory postsynaptic current
EPSP	excitatory postsynaptic potential
IPSC	inhibitory postsynaptic current

References

Atwood HL, Karunanithi S. Diversification of synaptic strength: presynaptic elements. Nat Rev Neurosci. 2002; 3:497–516. [PubMed: 12094207]

Banke TG, McBain CJ. GABAergic input onto CA3 hippocampal interneurons remains shunting throughout development. J Neurosci. 2006; 26(11):720–11. 725.

Buzsaki G. Feed-forward inhibition in the hippocampal formation. Prog Neurobiol. 1984; 22:131–153. [PubMed: 6433403]

Debanne D, Guerineau NC, Gahwiler BH, Thompson SM. Physiology and pharmacology of unitary synaptic connections between pairs of cells in areas CA3 and CA1 of rat hippocampal slice cultures. J Neurophysiol. 1995; 73:1282–1294. [PubMed: 7608771]

Debanne D, Thompson SM, Gahwiler BH. A brief period of epileptiform activity strengthens excitatory synapses in the rat hippocampus in vitro. Epilepsia. 2006; 47:247–256. [PubMed: 16499748]

Gabernet L, Jadhav SP, Feldman DE, Carandini M, Scanziani M. Somatosensory integration controlled by dynamic thalamocortical feed-forward inhibition. Neuron. 2005; 48:315–327. [PubMed: 16242411]

Geiger JR, Lubke J, Roth A, Frotscher M, Jonas P. Submillisecond AMPA receptor-mediated signaling at a principal neuron-interneuron synapse. Neuron. 1997; 18:1009–1023. [PubMed: 9208867]

Golowasch J, Goldman MS, Abbott LF, Marder E. Failure of averaging in the construction of a conductance-based neuron model. J Neurophysiol. 2002; 87:1129–1131. [PubMed: 11826077]

Holmgren C, Harkany T, Svennenfors B, Zilberter Y. Pyramidal cell communication within local networks in layer 2/3 of rat neocortex. J Physiol. 2003; 551:139–153. [PubMed: 12813147]

Karnup S, Stelzer A. Temporal overlap of excitatory and inhibitory afferent input in guinea-pig CA1 pyramidal cells. J Physiol. 1999; 516 (2):485–504. [PubMed: 10087347]

Klyachko VA, Stevens CF. Excitatory and feed-forward inhibitory hippocampal synapses work synergistically as an adaptive filter of natural spike trains. PLoS Biol. 2006; 4:e207. [PubMed: 16774451]

Koester HJ, Johnston D. Target cell-dependent normalization of transmitter release at neocortical synapses. Science. 2005; 308:863–866. [PubMed: 15774725]

Lamsa K, Heeroma JH, Kullmann DM. Hebbian LTP in feed-forward inhibitory interneurons and the temporal fidelity of input discrimination. Nat Neurosci. 2005; 8:916–924. [PubMed: 15937481]

Lien CC, Mu Y, Vargas-Caballero M, Poo MM. Visual stimuli-induced LTD of GABAergic synapses mediated by presynaptic NMDA receptors. Nat Neurosci. 2006; 9:372–380. [PubMed: 16474391]

Lloyd DPC. Facilitation and inhibition of spinal motoneurons. J Neurophysiol. 1946; 9:421–438. [PubMed: 20274399]

MacLean JN, Zhang Y, Johnson BR, Harris-Warrick RM. Activity-independent homeostasis in rhythmically active neurons. Neuron. 2003; 37:109–120. [PubMed: 12526777]

Maffei A, Nelson SB, Turrigiano GG. Selective reconfiguration of layer 4 visual cortical circuitry by visual deprivation. Nat Neurosci. 2004; 7:1353–1359. [PubMed: 15543139]

Miles R. Synaptic excitation of inhibitory cells by single CA3 hippocampal pyramidal cells of the guinea-pig in vitro. J Physiol (Lond). 1990; 428:61–77. [PubMed: 2231426]

Miles R, Wong RK. Excitatory synaptic interactions between CA3 neurones in the guinea-pig hippocampus. J Physiol. 1986; 373:397–418. [PubMed: 3018233]

Mittmann W, Koch U, Hausser M. Feed-forward inhibition shapes the spike output of cerebellar Purkinje cells. J Physiol. 2005; 563:369–378. [PubMed: 15613376]

Pavlidis P, Madison DV. Synaptic transmission in pair recordings from CA3 pyramidal cells in organotypic culture. J Neurophysiol. 1999; 81:2787–2797. [PubMed: 10368397]

Pouille F, Scanziani M. Enforcement of temporal fidelity in pyramidal cells by somatic feed-forward inhibition. Science. 2001; 293:1159–1163. [PubMed: 11498596]

Reyes A, Lujan R, Rozov A, Burnashev N, Somogyi P, Sakmann B. Target-cell-specific facilitation and depression in neocortical circuits. Nat Neurosci. 1998; 1:279–285. [PubMed: 10195160]

Schweizer FE, Dresbach T, DeBello WM, O'Connor V, Augustine GJ, Betz H. Regulation of neurotransmitter release kinetics by NSF. Science. 1998; 279:1203–1206. [PubMed: 9469810]

Simons DJ, Carvell GE. Thalamocortical response transformation in the rat vibrissa/barrel system. J Neurophysiol. 1989; 61:311–330. [PubMed: 2918357]

Stoppini L, Buchs PA, Muller D. A simple method for organotypic cultures of nervous tissue. J Neurosci Meth. 1991; 37:173–182.

Sugino K, Hempel CM, Miller MN, Hattox AM, Shapiro P, Wu C, Huang ZJ, Nelson SB. Molecular taxonomy of major neuronal classes in the adult mouse forebrain. Nat Neurosci. 2006; 9:99–107. [PubMed: 16369481]

Tao HW, Poo MM. Activity-dependent matching of excitatory and inhibitory inputs during refinement of visual receptive fields. Neuron. 2005; 45:829–836. [PubMed: 15797545]

Toyoizumi T, Pfister JP, Aihara K, Gerstner W. Generalized Bienenstock-Cooper-Munro rule for spiking neurons that maximizes information transmission. Proc Natl Acad Sci USA (PNAS). 2005; 102:5239–5244.

Turrigiano GG, Nelson SB. Homestatic plasticity in the developing nervous system. Nat Rev Neurosci. 2004; 5:97–107. [PubMed: 14735113]

Wang Y, Markram H, Goodman PH, Berger TK, Ma J, Goldman-Rakic PS. Heterogeneity in the pyramidal network of the medial prefrontal cortex. Nat Neurosci. 2006; 9:534–542. [PubMed: 16547512]

Wehr M, Zador AM. Balanced inhibition underlies tuning and sharpens spike timing in auditory cortex. Nature. 2003; 426:442–446. [PubMed: 14647382]

Wilent WB, Contreras D. Dynamics of excitation and inhibition underlying stimulus selectivity in rat somatosensory cortex. Nat Neurosci. 2005; 8:1364–1370. [PubMed: 16158064]

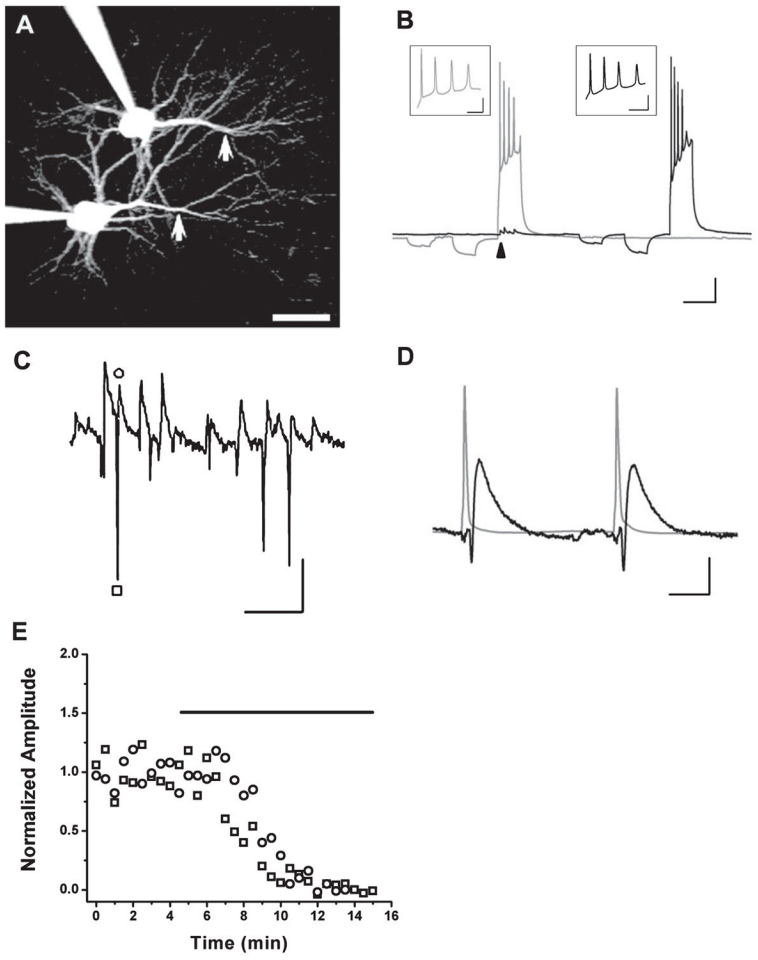

Fig. 1.

Whole-cell patch-clamp recordings of CA3 pyramidal cells reveal the presence of mixed excitatory–inhibitory responses. (A) Two-photon image (maximal intensity projection of a z-stack of 15 images taken at 3 μm intervals) of a pair of synaptically connected CA3 pyramidal cells that were filled with fluorescent dye Alexa-594 (25 μm) during a patch-clamp recording. The main apical dendrites (arrows) and multiple basal dendrites can be clearly seen extending out of the triangular-shaped cell body. Scale bar, 10 μm. (B) In current clamp, long-depolarizing pulses elicit a regular, accommodating spiking pattern in these cells. The first depolarization in this dual recording elicits a train of APs in the presynaptic neuron [gray trace that evokes a train of EPSPs (arrow) in the synaptically connected neighbor (black trace)]. Two hyperpolarizing pulses of different amplitudes were given before the depolarizations to monitor the cells' passive properties. Inset: Magnified view of the pattern of APs. Scale bar: 15 mV/150 ms; inset, 50 mV/15 ms. (C) Spontaneous activity recorded at a membrane potential close to −50 mV shows that many of the postsynaptic currents are a mixture of an early monosynaptic excitatory response (□) followed by an outward inhibitory response (○). Scale bar, 30 pA/250 ms. (D) These mixed synaptic responses (black trace) were also found when they were evoked by eliciting an AP in a neighboring presynaptic cell (gray trace). Scale bar, 25 mV/25 ms and 25 pA/25 ms. (E) Addition of 20 μm 6,7-dinitroquinoxaline-2,3-dione to the extracellular bath solution (indicated by bar) blocked this mixed evoked responses [excitatory (□) and inhibitory (○) response].

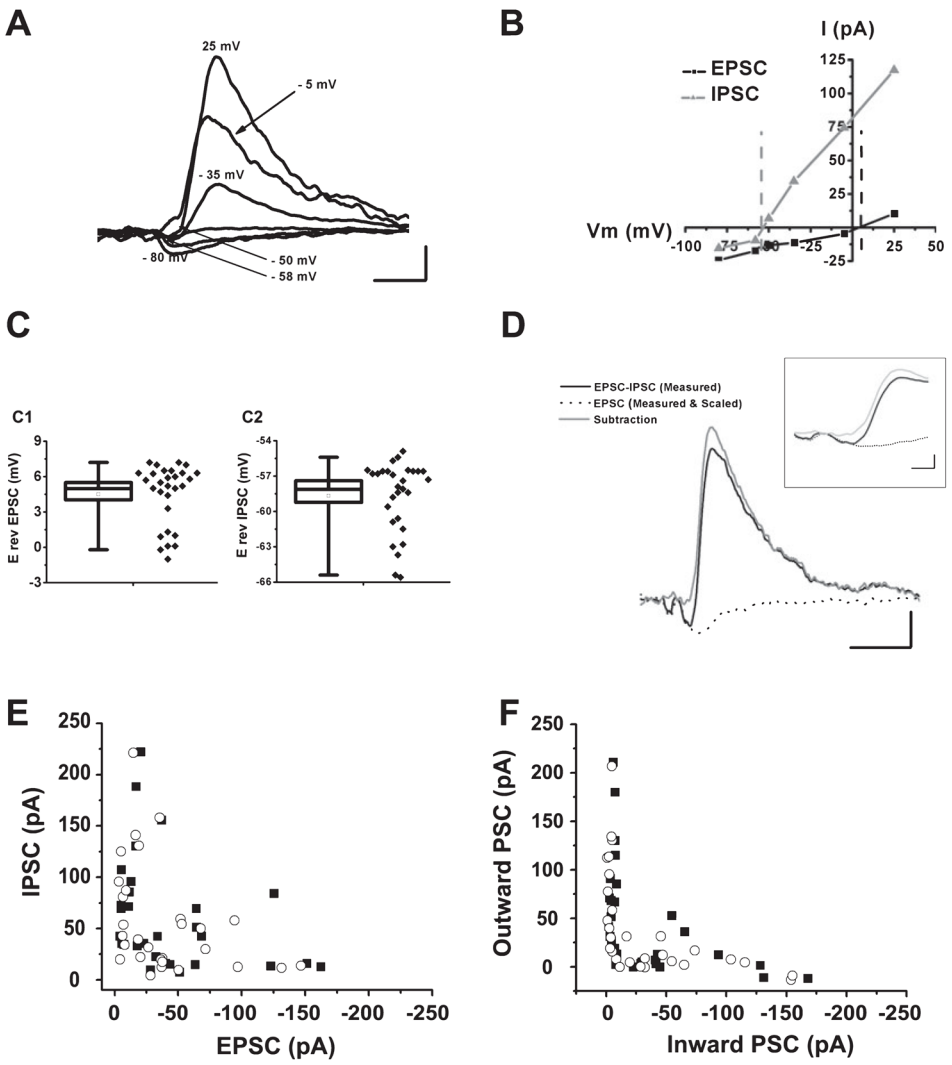

Fig. 2.

Simultaneous recordings from pairs of CA3 pyramidal neurons reveal a lack of correlation between excitatory and inhibitory current amplitudes. (A) Examples of postsynaptic currents (PSCs) that were evoked at a range of membrane potentials (V_m). Scale bar, 15pA/15 ms. (B) The peak inward (black) and outward (gray) current amplitudes of traces in A were measured and plotted against the holding potential V_m. These traces were used to find the E_{rev} for the individual currents in the mixed response. Dotted lines in the I–V plot indicate the interpolated reversal potential of excitation (black; E_{rev} EPSC) and inhibition (gray; Erev IPSC). Bar graph (and individual data to the right) of the reversal potentials for excitation (C1) and inhibition (C2) for all experiments (□, mean; box, ± SEM; horizontal line in box, median; whiskers, 10–90% values). (D) Isolation of EPSC and IPSC. A mixed E–I postsynaptic current was measured at −50 mV (black trace). The 'pure' EPSC trace was then recorded at E_{rev} IPSC and scaled to account for the different driving force at −50 mV (dotted trace). Subtraction of the scaled 'pure' EPSC (dotted trace) from the mixed EPSC (black trace) yielded the pure IPSC (gray trace). Scale bar, 15 pA/15 ms. Inset: Onset at higher magnification. Scale bar, 15 pA/2.5 ms. (E) Plot of IPSC amplitude against EPSC amplitude (determined as described in D) for all experiments reveals a non-random distribution (i.e. EPSCs of larger amplitude are accompanied by smaller IPSC and vice

versa), indicating that excitation and inhibition are not balanced (■, first response; ○, second response). (F) Plot of maximal outward currents against maximal inward currents measured at −50 mV (■, first response; ○, second response). Comparison with E highlights that the interaction of excitatory and inhibitory conductances enhances the segregation of weak and strong inputs.

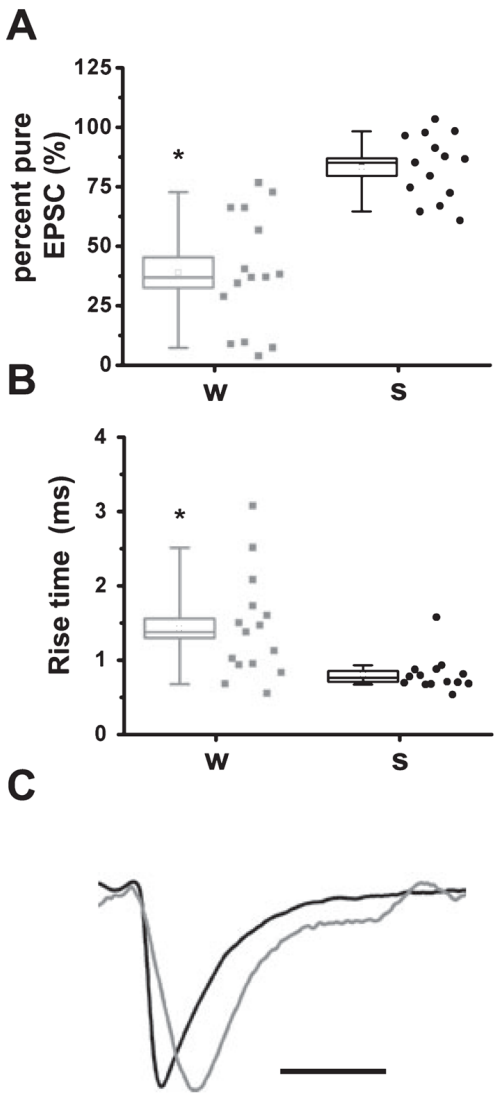

Fig. 3.

The EPSC of weak inputs is more efficiently occluded by feed-forward inhibition than the EPSC of strong inputs. (A) Percentage of inward current amplitude measured at −50 mV relative to the amplitude expected from then recording at E_{rev} IPSC (percent of pure EPSC) for weak (gray) and strong (black) responses (*$P < 0.05$). Inward currents of weak connections deviate more from the expected amplitude because of their effective occlusion by the larger IPSC (□, mean; box, ± SEM; horizontal line in box, median; whiskers, 10–90% values; individual data shown to the right of box). (B) Plot of the EPSC rise times for weak (gray) and strong (black) responses indicates that stronger inputs have faster rise times and thus potentially a greater contribution to the excitability of the postsynaptic membrane (□, mean; box, ± SEM; horizontal line in box, median; whiskers, 10–90% values; individual data shown to the right of box; *$P < 0.05$). (C) Typical response for weak (gray trace) and strong (black trace) inputs, normalized to peak amplitude. Scale bar, 15 ms. S, strong input; W, weak input.

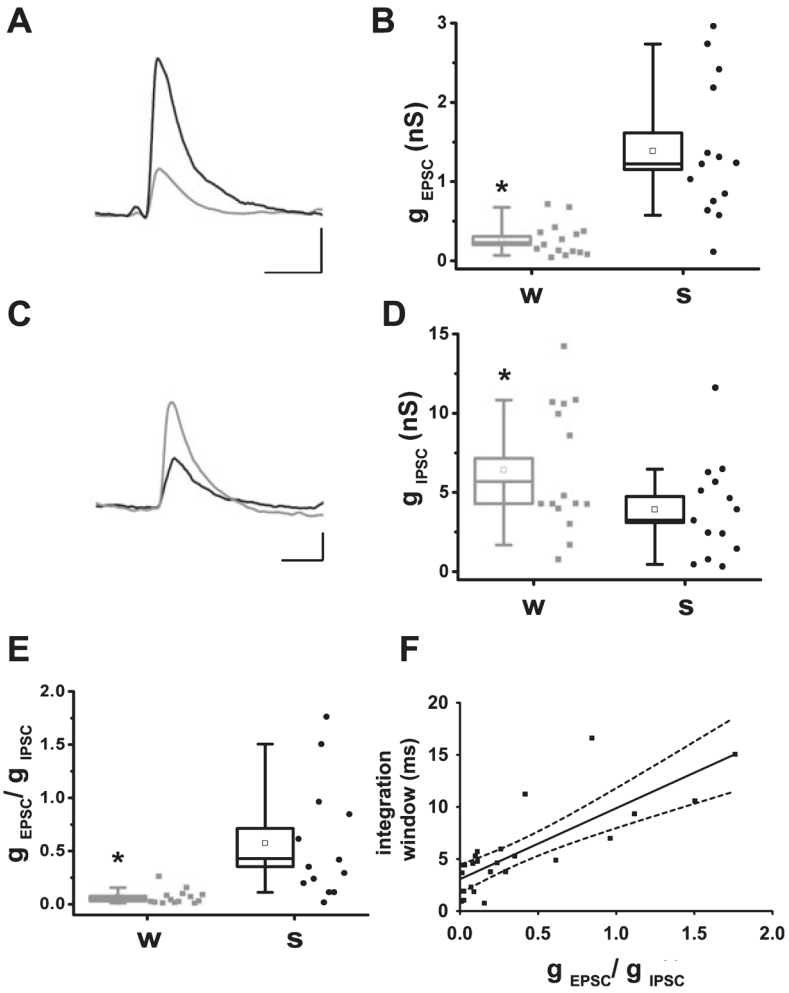

Fig. 4.

Isolation of conductances shows that weak and strong inputs have different excitation to inhibition ratios. (A) Example of excitatory conductance traces representative of weak (gray trace) and strong (black trace) inputs. Scale bar, 0.5 nS/25 ms. (B) Plot of both weak (gray) and strong (black) excitatory conductances (**P* < 0.05). (C) Example of inhibitory conductance traces representative of weak (gray trace) and strong (black trace) inputs. Scale bar, 3 nS/25 ms. (D) Plot of both weak (gray) and strong (black) inhibitory conductances. (E) Ratio of excitatory to inhibitory conductances for weak and strong inputs, respectively, demonstrating that the two inputs have significantly distinct excitation: inhibition ratios (**P* < 0.05). (F) This relationship can also be shown by plotting the integration window vs. the ratio of excitation to inhibition. The integration window was measured as the time between the start of the inward current and the start of the outward current ($R = 0.78$; $P < 0.05$). S, strong input; W, weak input.

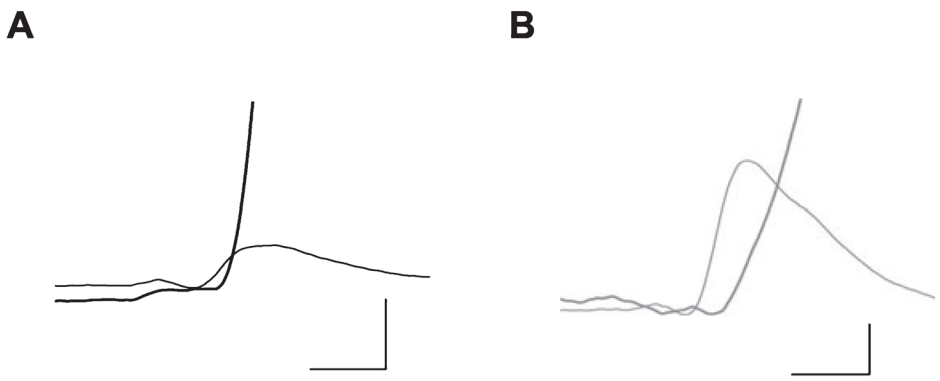

Fig. 5.

Weak and strong inputs have different temporal dynamics between excitation and inhibition. (A) Average traces indicating that, in weak inputs (black traces), the slow EPSC conductance (thin trace) is quickly occluded by the IPSC conductance (thick trace). (B) Average traces showing that, in strong inputs (gray traces), the faster kinetics of the EPSC (thin trace) result in more excitation of the postsynaptic membrane before inhibition is recruited (thin trace). Scale bar, 0.5 nS/10 ms.

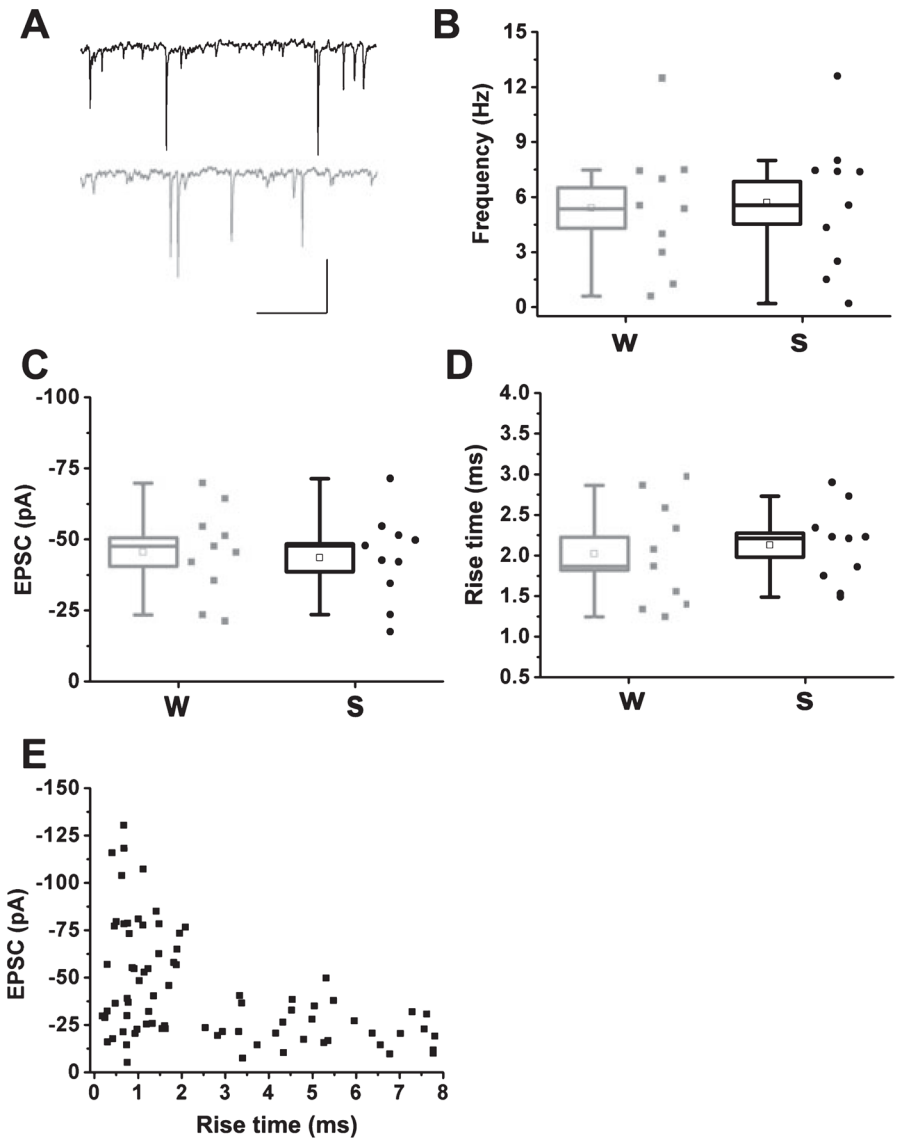

Fig. 6.

Postsynaptic cells do not differ in their spontaneous activity levels. (A) Sample traces for spontaneous activity of postsynaptic neurons that receive weak (top, black) or strong (bottom, gray) inputs when the presynaptic neuron is stimulated. (B) The frequency of the spontaneous activity was not different between the two neurons. (C and D) In addition, the amplitude and 20–80% rise time of these events were the same. These experiments suggest that the cells that we recorded from belong to a homogeneous population of pyramidal cells (□, mean; box, ± SEM; horizontal line in box, median; whiskers, 10–90% values; individual data shown to the right of box). (E) Plot of rise time against amplitude for spontaneous activity recorded during a voltage-clamp experiment. The segregation of weak and strong inputs is also evident in this L-shaped distribution; however, this distribution was not observed for all cell recordings. S, strong input; W, weak input.

Table 1

AP properties of pyramidal cells receiving weak or strong input

Pyramidal cells	Amplitude (mV)	Max. rate of depolarization (V/s)	Max. rate of repolarization (V/s)	Half width (ms)	Frequency (s^{-1})	Accommodation ratio
Weak input	96.06 ± 0.94	401.88 ± 4.97	−75.20 ± 1.56	2.02 ± 0.01	32.26 ± 1.58	2.36 ± 0.20
Strong input	98.63 ± 1.44	415.13 ± 6.97	−72.64 ± 1.18	2.06 ± 0.02	28.17 ± 2.85	2.81 ± 0.23
P-value	0.14	0.14	0.21	0.10	0.21	0.15

Values are means ± SEM of AP trains elicited by a 400 pA current injection (weak, n = 13 cells; strong, n = 16 cells). The frequency was calculated as the inverse of the average spike interval. The accommodation ration is calculated as the ratio of the last over the first interspike interval in a train.